Journal of Sound and Vibration (2000) **230**(2), 261–289
doi:10.1006/jsvi.1999.2615, available online at http://www.idealibrary.com on IDEAL®

THE EFFECTS OF PLANT AND DISTURBANCE UNCERTAINTIES IN ACTIVE CONTROL SYSTEMS ON THE PLACEMENT OF TRANSDUCERS

K. H. BAEK

Department of Mechanical Engineering, Dankook University, South Korea

AND

S. J. ELLIOTT

Institute of Sound and Vibration Research, University of Southampton, Southampton SO17 1 BJ, England

(*Received* 10 *December* 1998, *and in final form* 13 *July* 1999)

Previous studies of active control systems have shown that the overall performance could be greatly improved by optimizing the transducer positions. The robustness of such an optimized control system is investigated here for both unstructured, i.e., random, changes in the control environment, and for structured changes, such as those due to the presence of acoustical diffracting objects in an enclosure, for example. The study concentrates on how to simply describe the changes which occur in the plant response and disturbance in practice, and investigates how the cost function used in transducer positioning optimization techniques can be modified so that the performance is least affected by these changes. Mathematical and numerical analyses are used to help understand the overall robustness of an active control system to uncertainties in the plant response and disturbance. It is found that the degradation in performance due to small random changes in the disturbance is not affected by transducer location, whereas the degradation due to small random changes in the plant response does depend on transducer location. The effects of diffracting objects in an enclosure are analyzed in terms of the changes in the singular-value matrix of the nominal plant response, in which the objects are not present. Theoretical analysis showed that transducer positions with low control effort are generally good choices for robust performance. Several fitness functions were tested for use in the search for the optimum transducer locations and the results showed that use of the proper fitness function can effectively filter out the actuator positions with high control effort and can select transducer positions which can perform robustly.

1. INTRODUCTION

An important question in the practical application of active control is how to choose the "best" set of positions for the actuators and sensors from a much larger number of possible locations. The "best" can be defined as the maximization of a fitness function which should reflect the performance achieved by the selected

0022-460X/00/070261 + 29 $35.00/0

transducers in reducing the overall level of the sound or vibration. Many studies of this problem have been carried out, which often used natural algorithms to find optimal transducer locations, see for example references [1–7]. It has been found that if they are carefully implemented, both genetic algorithms and simulated annealing can give near-optional solutions to this problem by searching only a very small fraction of the total number of possible combinations [5]. The applications of such techniques to a laboratory experiment [5] and a helicopter [8] showed that the overall performance of an active control system can be greatly improved by adjusting the transducer positions and that the correct transducer positioning can be as important as the control algorithm itself. Although the predicted performance could be much improved by the careful selection of transducer positions, it was unclear whether these selected positions would still perform well in practice, when there are changes in the control environment due for example to changes in temperature, frequency, etc. The robustness of this achieved performance may be dependent on the type of uncertainties in the plant response and primary disturbance. The problem dealt with in this paper is concerned with the effect of such uncertainties on the active control system performance, especially related to the transducer positioning. Some initial results in this area were presented in reference [9]. One of the objects of this study is to examine how to simply describe the changes which occur in the plant response and disturbance in practice, and to investigate how the fitness function used in the transducer search algorithm can be modified so that the performance is least affected by these changes.

The uncertainty in either the plant or disturbance can be categorized into structured and unstructured forms. There are two distinct problems for the modelling of uncertainty in the plant. The first is when there is a modelling error in the plant response estimation and the second is when the estimation of the plant accurately represents the physical plant in a nominal state but the response of the physical plant varies from the nominal state. The problem dealt with in this study is the second case, uncertainty in the physical plant response.

In the unstructured uncertainty case, the variations in each element of the disturbance vector or plant matrix are assumed to be independent of each other, which is typical of the unstructured uncertainties associated with measurement errors, for example. On the other hand, for structured uncertainties, the changes in the elements of the disturbance vector and plant matrix are dependent upon each other and so the matrix of changes has a certain structure. Structured uncertainties in the plant response and the disturbance occur as a result of physical changes in the system under control, caused, for example, by the presence or absence of passengers in an actively controlled enclosure. The magnitude of these changes can be much larger than the unstructured measurement errors discussed above. In this study, the effects of such acoustical diffracting objects are modelled using the equivalent source method (ESM) [10]. The effects of diffracting spheres in the enclosure are analysed in terms of the changes in the singular-value matrix of the nominal plant response, in which the spheres are not present. Some measurements are also made with acoustic diffracting objects inside an experimental enclosure and when analyzed in the same way, these showed the same structure of uncertainty as was predicted from the theoretical model. The selection of robust transducer

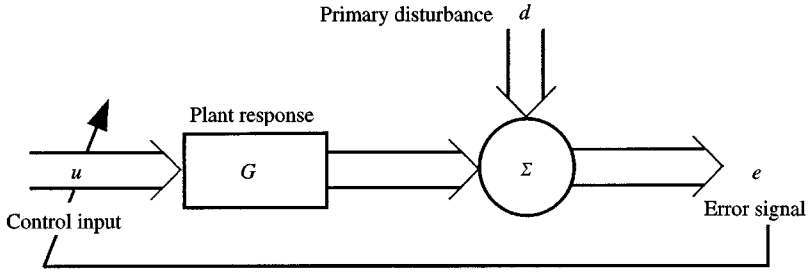

Figure 1. Block diagram of the active control system.

positions is also considered for various cases of structured uncertainty in the plant response and disturbance vector.

Several fitness functions are tested for use in natural algorithms, which can be used to efficiently search the huge combinatorial problem of selecting a large number of transducer positions from a much larger set of possible locations. In this paper, the simulated annealing algorithm was used to choose the best sets of positions for the actuators and sensors when there were uncertainties in both the disturbance and the plant.

2. UNSTRUCTURED UNCERTAINTY IN THE PLANT RESPONSE AND DISTURBANCE

Figure 1 shows a typical block diagram of a pure tone multichannel feedforward active noise control system. For a single-frequency excitation with a given set of actuators and sensors, the complex vector of L steady state error signals $\mathbf{e}$ can be expressed in a vector form as

$$\mathbf{e} = \mathbf{d} + \mathbf{G}\mathbf{u}, \tag{1}$$

where $\mathbf{G}$ is an $(L \times M)$ plant response matrix, $\mathbf{d}$ is a primary disturbance vector and $\mathbf{u}$ is the vector of M complex inputs to the secondary sources. For the overdetermined case, $L > M$, the optimum input vector signal which minimizes the sum of squared errors, $\mathbf{e}^{\mathrm{H}}\mathbf{e}$, is given by

$$\mathbf{u}_{\mathrm{opt}} = -[\mathbf{G}^{\mathrm{H}}\mathbf{G}]^{-1}\mathbf{G}^{\mathrm{H}}\mathbf{d}, \tag{2}$$

where the superscript H denotes the Hermitian, i.e., complex conjugate, transpose of a vector or matrix.

The minimum residual value of the sum of squared errors is then given by

$$J_{\min} = \mathbf{d}^{\mathrm{H}}[\mathbf{I} - \mathbf{G}[\mathbf{G}^{\mathrm{H}}\mathbf{G}]^{-1}\mathbf{G}^{\mathrm{H}}]\mathbf{d} \tag{3}$$

and the resulting dB attenuation in the sum of the mean-square error signals is

$$Attn = -10\log_{10}(\mathbf{e}_{\min}^{\mathrm{H}}\mathbf{e}_{\min}/\mathbf{d}^{\mathrm{H}}\mathbf{d}). \tag{4}$$

The control effort required to achieve this attenuation is defined to be the sum of squared actuator signals which is

$$Effort = \mathbf{u}_{\mathrm{opt}}^{\mathrm{H}}\mathbf{u}_{\mathrm{opt}}. \tag{5}$$

If the cost function being minimized is modified to include a degree of effort weighting, so that it becomes $\mathbf{e}^{\mathrm{H}}\mathbf{e} + \beta\mathbf{u}^{\mathrm{H}}\mathbf{u}$ for example, then the optimum input vector and minimum cost function have the same form as equations (2) and (3) but $[\mathbf{G}^{\mathrm{H}}\mathbf{G}]^{-1}$ is replaced by $[\mathbf{G}^{\mathrm{H}}\mathbf{G} + \beta\mathbf{I}]^{-1}$.

Transducers in the "best" positions for an active noise control system are not only those which maximize noise reductions, but they must also maintain robust performance to certain realistic uncertainties in the plant response and the primary disturbance. We now assume that the response of the physical plant $\mathbf{G}_p$ can vary from the nominal state $\mathbf{G}_0$. We can relate the physical plant and nominal state by

$$\mathbf{G}_p = \mathbf{G}_0 + \Delta\mathbf{G}, \tag{6}$$

where $\Delta\mathbf{G}$ is the uncertainty in the plant response. The amount of uncertainty in the plant response is quantified here as being

$$\varepsilon_1 = \frac{E[\,\|\Delta\mathbf{G}\|_F]}{\|\mathbf{G}_0\|_F}, \tag{7}$$

where E denotes the expectation over the random variables in $\Delta\mathbf{G}$ and $\|\mathbf{G}_0\|_F$ is the Frobenius of Euclidian norm defined by

$$\|\mathbf{G}_0\|_F = \left(\sum_{l=1}^{L}\sum_{m=1}^{M}|G_{lm}|^2\right)^{1/2}. \tag{8}$$

Similarly, the uncertainty in the disturbance can be modelled as

$$\mathbf{d}_p = \mathbf{d}_0 + \Delta\mathbf{d}, \tag{9}$$

where $\mathbf{d}_p$ is the disturbance with uncertainty, $\mathbf{d}_0$ is the nominal disturbance and $\Delta\mathbf{d}$ is the random uncertainty in the disturbance. The amount of uncertainty in the disturbance is quantified here as being

$$\varepsilon_2 = \frac{E[\,\|\Delta\mathbf{d}\|_2]}{\|\mathbf{d}_0\|_2}. \tag{10}$$

The definitions given in equations (7) and (10) are used to provide a normalized measure for both structured and unstructured uncertainties.

2.1. UNSTRUCTURED UNCERTAINTY IN DISTURBANCE

If the uncertainty consists of independent random perturbations in each element it is said to be unstructured and if it exists only in the disturbance, then

$$\mathbf{d} = \mathbf{d}_0 + \Delta\mathbf{d} \tag{11}$$

and

$$\mathbf{G} = \mathbf{G}_0. \tag{12}$$

Assume $\Delta\mathbf{d}$ has zero mean,

$$E[\Delta\mathbf{d}] = 0, \tag{13}$$

so that

$$E[\Delta\mathbf{d}^{\mathrm{H}}\mathbf{d}_0] = 0 \tag{14}$$

and

$$E[\Delta\mathbf{d}^{\mathrm{H}}\mathbf{A}\mathbf{d}_0] = 0 \tag{15}$$

for any $\mathbf{A}$.

The minimum residual error $J_{\min}$ is

$$J_{\min} = (\mathbf{d}_0^{\mathrm{H}} + \Delta\mathbf{d}^{\mathrm{H}})[\mathbf{I} - \mathbf{G}_0(\mathbf{G}_0^{\mathrm{H}}\mathbf{G}_0)^{-1}\mathbf{G}_0^{\mathrm{H}}](\mathbf{d}_0 + \Delta\mathbf{d}) \tag{16}$$

which can be written as

$$J_{\min} = \mathbf{d}_0^{\mathrm{H}}\mathbf{A}\mathbf{d}_0 + \mathbf{d}_0^{\mathrm{H}}\mathbf{A}\Delta\mathbf{d} + \Delta\mathbf{d}^{\mathrm{H}}\mathbf{A}\mathbf{d}_0 + \Delta\mathbf{d}^{\mathrm{H}}\mathbf{A}\Delta\mathbf{d}, \tag{17}$$

where

$$\mathbf{A} = \mathbf{I} - \mathbf{G}_0(\mathbf{G}_0^{\mathrm{H}}\mathbf{G}_0)^{-1}\mathbf{G}_0^{\mathrm{H}} \tag{18}$$

is a positive-definite matrix.

The mean value of $J_{\min}$ is thus given by the expectation

$$E[J_{\min}] = \mathbf{d}_0^{\mathrm{H}}\mathbf{A}\mathbf{d}_0 + E[\Delta\mathbf{d}^{\mathrm{H}}\mathbf{A}\Delta\mathbf{d}], \tag{19}$$

where equation (15) has been used to simplify the expression, which may be written as

$$E[J_{\min}] = J_0 + E[\Delta J], \tag{20}$$

where

$$J_0 = \mathbf{d}_0^{\mathrm{H}}\mathbf{A}\mathbf{d}_0 \tag{21}$$

is the minimum cost function if $\Delta\mathbf{d} = 0$, and

$$\Delta J = \Delta\mathbf{d}^{\mathrm{H}}\mathbf{A}\Delta\mathbf{d} \tag{22}$$

which must be positive since $\mathbf{A}$ is positive definite. Thus, the average attentuation, equation (4), is predicted to be consistently less than the attenuation with no uncertainty. The reduction in attenuation depends on $\mathbf{A}$, and hence on $\mathbf{G}$, and thus appears to depend on the actuator locations.

The matrix $\mathbf{A}$, which has a size of $L \times L$ if $\mathbf{G}_0$ has a size of $L \times M$ ($L > M$), can be expressed in terms of a unitary matrix $\mathbf{Q}$ and a diagonal matrix of eigenvalues, $\mathbf{\Lambda} = diag(\lambda_1, \lambda_2, \ldots, \lambda_L)$, where all eigenvalues are real, so that we can write

$$\mathbf{A} = \mathbf{Q}\mathbf{\Lambda}\mathbf{Q}^{\mathrm{H}}. \tag{23}$$

Let

$$\mathbf{p} = \mathbf{Q}^{\mathrm{H}}\Delta\mathbf{d}, \tag{24}$$

then

$$E[\Delta J] = E[\mathbf{p}^{\mathrm{H}}\mathbf{\Lambda}\mathbf{p}]. \tag{25}$$

Expressing $\mathbf{p}$ as $[p_1, p_2, \ldots, p_L]^{\mathrm{T}}$, $E[\Delta J]$ can be written as

$$E[\Delta J] = \sum_{i=l}^{L} \lambda_i E[|p_i|^2]. \tag{26}$$

If the elements of the vector $\Delta\mathbf{d}$ are independent random numbers with variance c, then the "covariance" matrix of $\Delta\mathbf{d}$ is

$$E[\Delta\mathbf{d}\Delta\mathbf{d}^{\mathrm{H}}] = c\mathbf{I}, \tag{27}$$

where c is the variance of the modulus of each element of $\Delta\mathbf{d}$, which, from equation (10), is equal to

$$c = \frac{1}{L}\varepsilon_2^2 \|d_0\|_2^2. \tag{28}$$

The covariance matrix for the vector $\mathbf{p}$ is also given by

$$E[\mathbf{p}\mathbf{p}^{\mathrm{H}}] = \mathbf{Q}^{\mathrm{H}}E[\Delta\mathbf{d}\Delta\mathbf{d}^{\mathrm{H}}]\mathbf{Q} = c\mathbf{I} \tag{29}$$

since $\mathbf{Q}$ is unitary. Thus, the elements of the vector $\mathbf{p}$ are also independent random numbers with the same variance as the elements of $\Delta\mathbf{d}$. Equation (26) can thus be written as

$$E[\Delta J] = \frac{1}{L}\varepsilon_2^2 \|\mathbf{d}_0\|_2^2 \sum_{i=1}^{L} \lambda_i = \frac{1}{L}\varepsilon_2^2 \|\mathbf{d}_0\|_2^2 \, trace(\mathbf{A}). \tag{30}$$

The eigenvalues λ_i of matrix $\mathbf{A}$, given by equation (18), have a rather special form which can be established by writing

$$\mathbf{A} = \mathbf{I} - \mathbf{C}, \tag{31}$$

where

$$\mathbf{C} = \mathbf{G}_0(\mathbf{G}_0^{\mathrm{H}}\,\mathbf{G}_0)^{-1}\mathbf{G}_0^{\mathrm{H}}. \tag{32}$$

Note that $\mathbf{C}$ is Hermitian and of rank M, and so has M non-zero eigenvalues, and also that

$$\mathbf{C}^n = \mathbf{C} \tag{33}$$

so that eigenvalues of $\mathbf{C}$, λ_c, must have the property of

$$\lambda_c^n = \lambda_c, \tag{34}$$

i.e., they must be either 0 or 1. Thus, $\mathbf{C}$ has M non-zero eigenvalues which must all be equal to unity. The trace of $\mathbf{A}$ is thus equal to

$$trace(\mathbf{A}) = trace(\mathbf{I}) - trace(\mathbf{C}) = L - M, \tag{35}$$

since the trace of the $(L \times L)$ unit matrix $\mathbf{I}$ is equal to L.

The final expression for the average excess mean-square error caused by the unstructured uncertainties in the disturbance vector takes the remarkably simple form

$$E[\Delta J] = \left(\frac{L - M}{L}\right)\varepsilon_2^2\,\|\mathbf{d}_0\|_2^2. \tag{36}$$

This equation implies that (1) for a given number of actuators (M) and sensors (L), $E[\Delta J]$ is independent of the choice of actuators and sensor position; (2) $E[\Delta J]$ is proportional to the total variance of $\Delta\mathbf{d}$; and (3) $E[\Delta J]$ is zero if the number of actuators is equal to the number of sensors ($L = M$) and increases in proportion to the relative difference between the number of sensors and number of actuators ($(L - M)/L$).

Since $E(\Delta J)$ is proportional to the variance of $\Delta\mathbf{d}$, the average attenuation achieved by the active control system must inevitably decrease when such perturbations are introduced into the disturbance vector due to the primary source, as recently observed by Martin and Gronier [11].

Figure 2 shows simulation results for $E(\Delta J)$ with 32 microphones averaged over 1000 cases of disturbance perturbation with a single set of loudspeakers, and the predicted value of $E\,(\Delta J)$ using equation (36). In general, the simulation results are in good agreement with the theory except when a small number of loudspeakers are used. This appears to be due to statistical errors caused by using a finite number of samples.

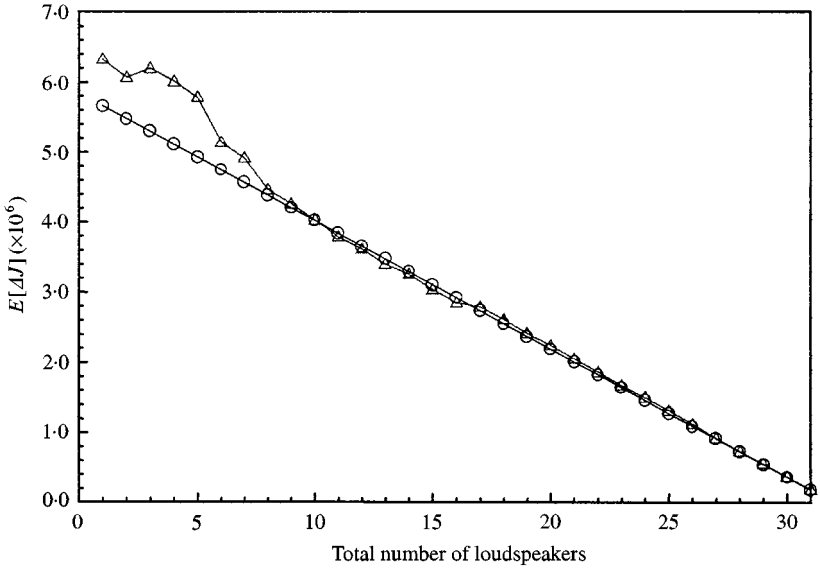

Figure 2. The effect of the total number of loudspeakers on $E[\Delta J]$ when there is 1% of unstructured uncertainty (i.e., $\varepsilon_2 = 0{\cdot}01$) in the disturbance. The simulation results are averaged over 1000 samples with 32 microphones: △–△–△, simulation; ○–○–○, theory.

2.2. UNSTRUCTURED UNCERTAINTY IN PLANT RESPONSE

If the uncertainty exist only in the plant response, then

$$\mathbf{G} = \mathbf{G}_0 + \Delta\mathbf{G} \tag{37}$$

and

$$\mathbf{d} = \mathbf{d}_0 \tag{38}$$

Assume $\Delta\mathbf{G}$ has zero mean,

$$E[\Delta\mathbf{G}] = 0, \tag{39}$$

so that

$$E[\Delta\mathbf{G}^{\mathrm{H}}\mathbf{G}_0] = 0 \tag{40}$$

and

$$E[\Delta\mathbf{G}^{\mathrm{H}}\mathbf{A}\mathbf{G}_0] = 0 \tag{41}$$

for any $\mathbf{A}$. Since elements of $\Delta\mathbf{G}$ are assumed to be uncorrelated, then

$$E[\Delta\mathbf{G}^{\mathrm{H}}\Delta\mathbf{G}] = \beta\mathbf{I}, \tag{42}$$

where, using equations (7) and (8), β is given by

$$\beta = \frac{1}{M}\varepsilon_1^2 \|\mathbf{G}_0\|_F^2. \tag{43}$$

The minimum residual error $J_{\min}$ is

$$J_{\min} = \mathbf{d}_0^{\mathrm{H}} \{\mathbf{I} - (\mathbf{G}_0 + \Delta\mathbf{G})[(\mathbf{G}_0 + \Delta\mathbf{G})^{\mathrm{H}}(\mathbf{G}_0 + \Delta\mathbf{G})]^{-1}(\mathbf{G}_0 + \Delta\mathbf{G})^{\mathrm{H}}\}\mathbf{d}_0. \quad (44)$$

Further assuming that $\|\Delta\mathbf{G}\|_F < \|\mathbf{G}_0\|_F$ and that $\mathbf{G}_0$ is not ill-conditioned then

$$E[J_{\min}] = \mathbf{d}_0^{\mathrm{H}} \{\mathbf{I} - \mathbf{G}_0(\mathbf{G}_0^{\mathrm{H}}\mathbf{G}_0 + \beta\mathbf{I})^{-1}\mathbf{G}_0^{\mathrm{H}} - E[\Delta\mathbf{G}[(\mathbf{G}_0 + \Delta\mathbf{G})^{\mathrm{H}}(\mathbf{G}_0 + \Delta\mathbf{G})]^{-1}\Delta\mathbf{G}^{\mathrm{H}}]\}\mathbf{d}_0, \quad (45)$$

i.e.,

$$E[J_{\min}] = J_\beta - E[\Delta J_G], \quad (46)$$

where

$$J_\beta = \mathbf{d}_0^{\mathrm{H}}[\mathbf{I} - \mathbf{G}_0[\mathbf{G}_0^{\mathrm{H}}\mathbf{G}_0 + \beta\mathbf{I}]^{-1}\mathbf{G}_0^{\mathrm{H}}]\mathbf{d}_0 \quad (47)$$

is the minimum cost function with an effort weighting term, $\beta\mathbf{I}$, and

$$E|\Delta J_G| = \mathbf{d}_0^{\mathrm{H}} E[\Delta\mathbf{G}[(\mathbf{G}_0 + \Delta\mathbf{G})^{\mathrm{H}}(\mathbf{G}_0 + \Delta\mathbf{G})]^{-1}\Delta\mathbf{G}^{\mathrm{H}}]\,\mathbf{d}_0 \quad (48)$$

which is also positive, but does not appear to have a simple analytic form.

The average attenuation thus will be reduced by the effective weighting term and by a term which depends on $\mathbf{G}_0$ and $\mathbf{d}_0$. The performance of sets of loudspeakers which give good attenuation with low control effort will be relatively insensitive to small values of β. This is because the term $\beta\mathbf{u}^{\mathrm{H}}\mathbf{u}$ will be small compared to the term $\mathbf{e}^{\mathrm{H}}\mathbf{e}$ in the general cost function discussed at the beginning of this section. Thus, it is these loudspeaker sets for which the performance is likely to be less sensitive to random variations in the response of the plant.

2.3. SIMULATION RESULTS WITH UNSTRUCTURED UNCERTAINTIES

For the example problem of selecting the best eight loudspeaker positions from a possible 32 locations to minimize the sum of squared outputs of 32 microphones, a set of plant responses, $\mathbf{G}_0$, and disturbances $\mathbf{d}_0$, was measured at 88 Hz in an enclosure, which has approximate dimensions of 2·1 m × 2·1 m × 6·0 m. Exhaustive search results are shown in Table 1 and are used as a reference, since they have been obtained without any uncertainties and using the nominal fitness function defined in equation (4). Robust loudspeaker positions are then sought for three cases: (1) uncertainty in the disturbance only, (2) uncertainty in the plant response only, and (3) uncertainty in both the disturbance and plant response.

For ensembles of possible disturbances and plant responses with a given set of actuators and sensors, the fitness function used by the search algorithm, which is used as a measure of the average performance, is defined to be

$$\overline{Attn} = -10\log_{10}\left(\sum_{i=1}^{I}\mathbf{e}_i^{\mathrm{H}}\mathbf{e}_i \Big/ \sum_{i=1}^{I}\mathbf{d}_i^{\mathrm{H}}\mathbf{d}_i\right), \quad (49)$$

TABLE 1

Rank ordering of exhaustive search results for the best 8 *loudspeaker locations from* 32 *to minimize sum of squared outputs of* 32 *microphones without uncertainty in the disturbance and plant response*

Rank order	Attn. (dB)	Control effort	Loudspeaker position (1, present; 0, not present)
1	34·00	1·16	11000000000000101010100000010100
2	33·65	1·90	11000000000010100110100000000100
3	33·60	1·30	11001100000000101010000000000100
4	32·97	1·22	11000000000010101010100000000100
5	32·94	1·55	11000000000000100110100000010100
6	32·93	0·39	01010001000000101010000000000101
7	32·84	0·38	01010000000000101010001000000101
8	32·64	0·41	01010000000000101010000010000101
9	32·62	1·59	11000010000001100010100000000100
10	32·61	0·28	01000000000000101010100010000101
11	32·57	1·53	11000000000001100010100000010100
12	32·56	1·59	11000000001001100010100000000100
13	32·56	0·29	01000000100000101010100000000101
14	32·56	1·55	11000000000001100010110000000100
15	32·56	1·58	11000000010001100010100000000100
16	32·55	1·30	11100000000001100010100000000100
17	32·53	1·41	11000000000000100010100000010101
18	32·44	0·61	11100000000000100010100000010100
19	32·35	1·45	11000000000001100011100000000100
20	32·15	0·68	11100000000000100010100100000100

where

$$\mathbf{e}_i^{\mathrm{H}}\mathbf{e}_i = \mathbf{d}_i^{\mathrm{H}}\,[\mathbf{I} - \mathbf{G}_i[\mathbf{G}_i^{\mathrm{H}}\mathbf{G}_i]^{-1}\mathbf{G}_i^{\mathrm{H}}]\mathbf{d}_i\,. \tag{50}$$

For the unstructured uncertainty case, six sets of $\mathbf{d}_i$ and $\mathbf{G}_i$ are generated by adding random variations to $\mathbf{d}_0$ and $\mathbf{G}_0$ and $\overline{Attn}$ defined by equation (49) is used as a fitness function in a simulated annealing search [5]. Tables 2–4 show the search results for each of the three cases where the level of uncertainty has been chosen to give approximately the same attenuation in each case. When the uncertainty is only in the disturbance (Table 2), the ranking is similar to that with no uncertainty (Table 1), as predicted in section 2.1. A similar set of actuator locations is chosen when there are small uncertainties in either the plant (Table 3) or both the plant and disturbance (Table 4) and these are a subset of those chosen for the nominal plant and disturbance (Table 1) which have relatively low control effort.

Figure 3 shows the probability distribution of the attenuation for the loudspeaker sets designated cases 1 and 6, with uncertainty in the disturbance only. Case 1 gives the best performance in the search without any consideration of the uncertainty (Table 1) and case 6 performs almost as well with no uncertainty, but

TABLE 2

Simulated annealing search results with unstructured uncertainty in the disturbance with $\varepsilon_2 = 0{\cdot}018$

With uncertainty		Loudspeaker position	Without uncertainty		Rank
Attn. (dB)	Effort	(1, present; 0, not present)	Attn. (dB)	Effort	(Table 1)
32·12	1·15	11000000000000101010100000010100	34·00	1·16	1
31·99	1·86	11000000000010100110100000000100	33·65	1·90	2
31·88	1·29	11001100000000101010000000000100	33·60	1·30	3
31·47	1·21	11000000000010101010100000000100	32·97	1·22	4
31·45	1·50	11000000000000100110100000010100	32·94	1·55	5
31·41	1·61	11000010000001100010100000000100	32·62	1·59	9
31·41	1·53	11000000000001100010100000010100	32·57	1·53	11
31·40	1·33	11100000000001100010100000000100	32·55	1·30	16
31·35	1·60	11000000001001100010100000000100	32·56	1·59	12
31·35	1·60	11000000010001100010100000000100	32·56	1·58	15

TABLE 3

Simulated annealing search results with unstructured uncertainty in the plant response with $\varepsilon_1 = 0{\cdot}0063$

With uncertainty		Loudspeaker position	Without uncertainty		Rank
Attn. (dB)	Effort	(1, present; 0, not present)	Attn. (dB)	Effort	(Table 1)
32·12	0·39	01010001000000101010000000000101	32·93	0·39	6
32·03	0·39	01010000000000101010001000000101	32·84	0·38	7
32·02	0·28	01000000000000101010100010000101	32·61	0·28	10
32·00	0·29	01000000100000101010100000000101	32·56	0·29	13
31·69	0·41	01010000000000101010000010000101	32·64	0·41	8
31·36	0·30	01000000100000101010100000000101	31·89	0·30	26
31·33	0·50	11100000000000100010100000010100	32·44	0·61	18
31·16	1·00	11000000000000101010100000010100	34·00	1·16	1
31·12	0·20	01100100000000101010000000000101	31·52	0·20	36
31·08	0·15	01100000000000110010000100000110	31·30	0·15	48

has low control effort. As the uncertainty increases, the average attenuation decreases and the deviation in the attenuation increases. The average performance of case 1 is better than case 6 for all levels of disturbance uncertainties however, as predicted in section 2.1. Figure 4 shows the probability distribution of attenuation for cases 1 and 6 with uncertainty in the plant response. The average performance of case 6 is now better than case 1 for an uncertainty of $\varepsilon_1 = 10^{-2}$, so that with this level of plant uncertainty the loudspeaker set in case 6 will perform better, on

TABLE 4

Simulated annealing search results with unstructured uncertainty in the disturbance and plant response with $\varepsilon_1 = \varepsilon_2 = 0{\cdot}0059$

With uncertainty		Loudspeaker position (1, present; 0, not present)	Without uncertainty		Rank
Attn. (dB)	Effort		Attn. (dB)	Effort	(Table 1)
32·07	0·38	01010001000000101010000000000101	32·93	0·39	6
32·04	0·38	01010000000000101010001000000101	32·84	0·38	7
31·88	0·28	01000000000000101010100010000101	32·61	0·28	10
31·75	0·29	01000000100000101010100000000101	32·56	0·29	13
31·74	0·40	01010000000000101010000010000101	32·64	0·41	8
31·42	1·06	11000000000000101010100000010100	34·00	0·16	1
31·37	0·54	11100000000000100010100000010100	32·44	0·61	18
31·34	0·20	01100100000000101010000000000101	31·52	0·20	36
31·29	0·49	10010000000000101010001000000101	31·89	0·49	25
31·18	0·22	01100100000000100110000000000101	31·48	0·22	37

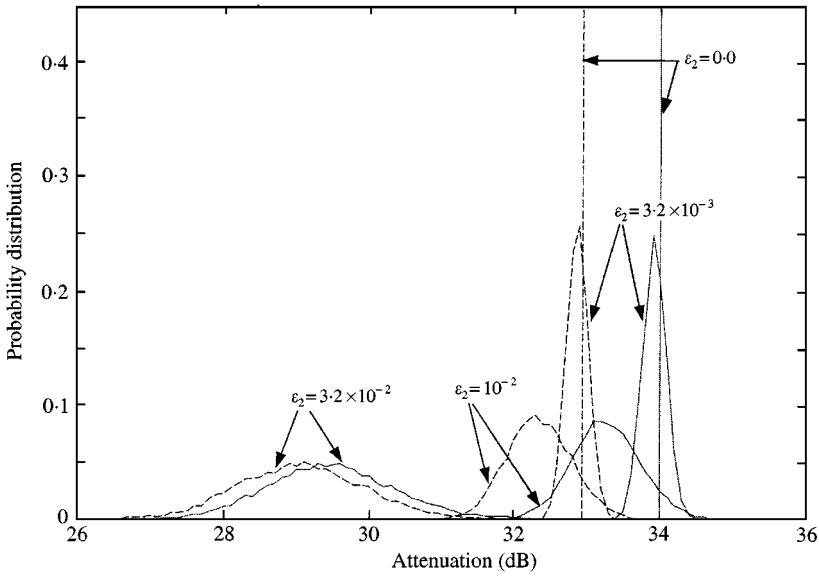

Figure 3. Probability distribution for attenuation with loudspeaker set case 1 (——) and case 6 (– – – –) with unstructured uncertainty in the disturbance.

average, than case 1, whereas with no uncertainty case 1 performs better than case 6. This is a crucial difference compared with Figure 3 and it again emphasizes the importance of choosing loudspeaker positions whose performance is robust to plant uncertainty, which are generally those which can give good performance with low control effort.

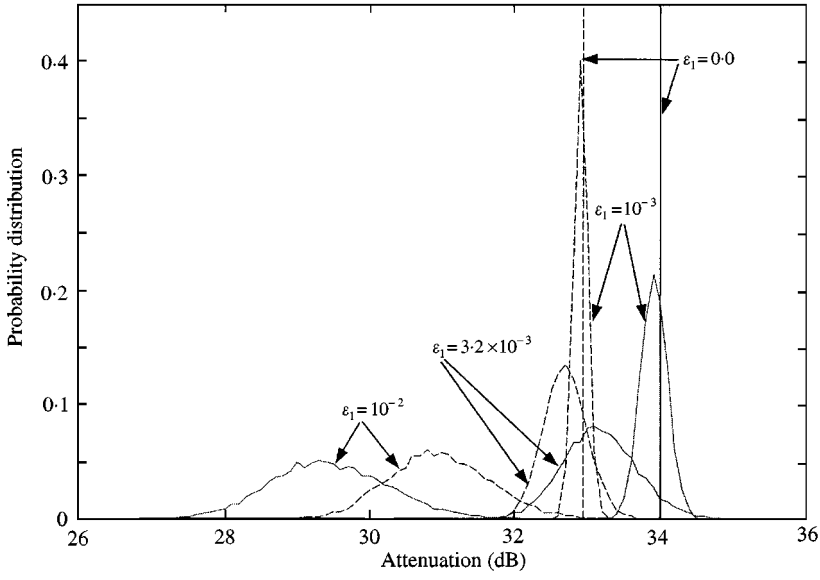

Figure 4. Probability distribution for attenuation with loudspeaker set case 1 (——) and case 6 (– – – –) with unstructured uncertainty in the plant response.

3. STRUCTURED UNCERTAINTY IN THE PLANT RESPONSE AND DISTURBANCE

In practical active sound control systems, much larger changes in the plant and the disturbance than those discussed above can occur as a result of physical changes in the space under control, caused, for example, by the presence or absence of passengers. The changes in the elements of the disturbance vector and plant matrix due to such changes are known to be dependent upon each other and so the uncertainty has a certain structure. The equivalent source method [10] has been used to model the effect of several acoustic diffracting objects on the plant response and disturbance vector in an enclosure. The effects of diffracting spheres in the enclosure are analyzed in terms of the changes in the singular-value matrix of the nominal plant response, in which the spheres are not present. Some measurements are also made with diffracting objects inside an experimental enclosure and these were analyzed in the same way. The selection of robust transducer positions was considered for various cases of structured uncertainty in the plant response and disturbance vector.

3.1. INTRODUCTION

In practice, some form of adaptive algorithm is used to adjust the inputs to the secondary sources in active control systems, which generally uses an internal model of the plant response. We will assume that this internal model is equal to the

nominal plant response, $\mathbf{G}_0$, and that the adaptive algorithm can be written in a generalized form as

$$\mathbf{u}(k+1) = \mathbf{u}(k) - \mathbf{M}\mathbf{G}_0^{\mathrm{H}}\mathbf{e}(k), \tag{51}$$

where $\mathbf{e}(k)$ is the measured error at the kth iteration. $\mathbf{G}_0^{\mathrm{H}}\mathbf{e}(k)$ is the assumed gradient of $\mathbf{e}^{\mathrm{H}}(k)\mathbf{e}(k)$ with respect to the real and imaginary parts of $\mathbf{u}$, and $\mathbf{M}$ is a positive-definite conditioning matrix which could be included to improve the convergence of the algorithm. $\mathbf{M}$ would be equal to $(\mathbf{G}_0^{\mathrm{H}}\mathbf{G}_0)^{-1}$ if an algorithm based on Newton's method were implemented, for example, and $\mathbf{I}$ for a steepest descent algorithm. The vector of measured error signals is assumed to be equal to

$$\mathbf{e}(k) = \mathbf{d} + \mathbf{G}_p\mathbf{u}(k), \tag{52}$$

where $\mathbf{G}_p$ is the response of the physical plant. Substituting equation (52) into equation (51) gives

$$\mathbf{u}(k+1) = \mathbf{u}(k) - \mathbf{M}[\mathbf{G}_0^{\mathrm{H}}\mathbf{d} + \mathbf{G}_0^{\mathrm{H}}\mathbf{G}_p\mathbf{u}(k)]. \tag{53}$$

Since the matrix $\mathbf{M}$ is positive definite, the steady state value of $\mathbf{u}(k)$, $\mathbf{u}_\infty$, for which $\mathbf{u}(k+1) = \mathbf{u}(k)$, must be given by setting the term in square bracket in equation (53) to zero, so that $\mathbf{u}_\infty$ must be given by

$$\mathbf{u}_\infty = -[\mathbf{G}_0^{\mathrm{H}}\mathbf{G}_p]^{-1}\mathbf{G}_0^{\mathrm{H}}\mathbf{d}, \tag{54}$$

assuming that $\mathbf{G}_0^{\mathrm{H}}\mathbf{G}_p$ is positive definite and that the algorithm is stable. Substituting equation (54) into equation (52) gives the steady state error, $\mathbf{e}_\infty$, for the adaptive algorithm in equation (51).

$$\mathbf{e}_\infty = [\mathbf{I} - \mathbf{G}_p[\mathbf{G}_0^{\mathrm{H}}\mathbf{G}_p]^{-1}\mathbf{G}_0^{\mathrm{H}}]\mathbf{d}. \tag{55}$$

Two other definitions of residual error signals are also used in this study which are

$$\mathbf{e}_0 = [\mathbf{I} - \mathbf{G}_0[\mathbf{G}_0^{\mathrm{H}}\mathbf{G}_0]^{-1}\mathbf{G}_0^{\mathrm{H}}]\mathbf{d}, \tag{56}$$

and

$$\mathbf{e}_p = [\mathbf{I} - \mathbf{G}_p[\mathbf{G}_p^{\mathrm{H}}\mathbf{G}_p]^{-1}\mathbf{G}_p^{\mathrm{H}}]\mathbf{d}. \tag{57}$$

For each case, the corresponding attenuations are defined as $Attn_\infty$, $Attn_0$ and $Attn_p$. The meaning of $Attn_0$ and $Attn_p$ are obvious from equations (55) and (56). $Attn_\infty$ indicates the attenuation achievable with an adaptive algorithm of the form of equation (51) having an internal model $\mathbf{G}_0$ acting on a physical plant, $\mathbf{G}_p$, with uncertainty.

Prior to the discussion of the selection of transducer positions, the effects of internal spheres in a room on the plant response are discussed here. The nominal plant matrix $\mathbf{G}_0$ can be decomposed into the form of

$$\mathbf{G}_0 = \mathbf{R}_0\mathbf{\Sigma}_0\mathbf{Q}_0^{\mathrm{H}}, \tag{58}$$

where $\mathbf{R}_0$ is the matrix of normalized eigenvectors of $\mathbf{G}_0\mathbf{G}_0^{\mathrm{H}}$, and $\mathbf{Q}_0$ is the matrix of normalized eigenvectors of $\mathbf{G}_0^{\mathrm{H}}\mathbf{G}_0$. The matrix $\mathbf{\Sigma}_0$ has the form of

$$\mathbf{\Sigma}_0 = \begin{bmatrix} \sigma_1 & 0 & \cdots & 0 \\ 0 & \sigma_2 & & \vdots \\ \vdots & & \ddots & \\ 0 & \cdots & & \sigma_M \\ 0 & \cdots & & 0 \\ \vdots & & & \vdots \\ 0 & \cdots & & 0 \end{bmatrix}, \tag{59}$$

where $\sigma_1, \sigma_2, \ldots, \sigma_M$ are the real singular values of $\mathbf{G}_0$. $\mathbf{\Sigma}_0$ has a size of $L \times M$ if $\mathbf{G}_0$ has a size of $L \times M$. If we define $\mathbf{\Sigma}_p$ as

$$\mathbf{\Sigma}_p = \mathbf{R}_0^{\mathrm{H}}\mathbf{G}_p\mathbf{Q}_0, \tag{60}$$

$\mathbf{G}_p$ can be expressed as

$$\mathbf{G}_p = \mathbf{R}_0\mathbf{\Sigma}_p\mathbf{Q}_0^{\mathrm{H}}. \tag{61}$$

This is a very similar form of equation (58) but, in this case, Σ_p will, in general, be a fully populated matrix. The changes of the singular-value matrix $\Delta\mathbf{\Sigma}$ due to the change $\Delta\mathbf{G}$ in the plant response can now be defined as

$$\begin{aligned} \Delta\mathbf{\Sigma} &= \mathbf{\Sigma}_p - \mathbf{\Sigma}_0 \\ &= \mathbf{R}_0^{\mathrm{H}}\mathbf{G}_p\mathbf{Q}_0 - \mathbf{R}_0^{\mathrm{H}}\mathbf{G}_0\mathbf{Q}_0 \\ &= \mathbf{R}_0^{\mathrm{H}}\Delta\mathbf{G}\,\mathbf{Q}_0. \end{aligned} \tag{62}$$

The importance of the $\Delta\mathbf{\Sigma}$ matrix on the stability and performance of active control systems has been discussed by Omoto and Elliott [12]. Different types of plant uncertainties can be identified since each type of uncertainty has its own pattern in the $\Delta\mathbf{\Sigma}$ matrix. The structure of the $\Delta\mathbf{\Sigma}$ matrix can also indicate the magnitude of the changes in the residual errors caused by variations in the plant response.

3.2. SIMULATION RESULTS USING ESM

Theoretical calculations of the plant response matrix and disturbance vector have been made using the equivalent source method (ESM) [10] for an active control system laboratory enclosure. The locations of the loudspeakers and microphones are sketched in Figure 5. For the ESM calculation at 88 Hz, the boundary conditions on the enclosure is matched using 26 image sources and 110 monopole equivalent sources distributed on the surface of a notional sphere of 100 m in diameter, as shown in Figure 6(a). Zero normal velocity boundary

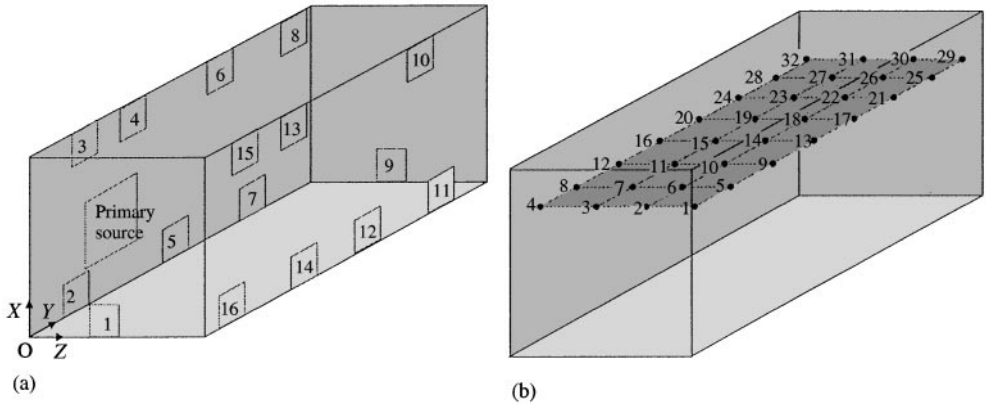

Figure 5. (a) Loudspeaker and (b) microphone positions in the laboratory enclosure. (The figures are not in exact scale and show only approximate positions.)

conditions are checked at 546 points uniformly distributed on the enclosure surface, which lie on the grid generated by dividing the X-, Y- and Z-axis into 7, 16 and 7 elements each. The secondary loudspeakers, are approximated as point monopole sources in the ESM calculations.

3.2.1. *The effect of numbers and size of sphere*

The plant response matrix is calculated for five cases, with and without a number of rigid spheres placed inside the enclosure, as shown in Figure 7. All spheres are modelled to have a diameter of 0·5 m except the large one shown in Figure 7(b), which has a diameter of 0·9 m and has approximately the same volume of six small spheres. The diameter of the small spheres was chosen so that their volume was approximately the same as a person weighing 65 kg. The schematic drawing for the modelling of small spheres is shown in Figure 6(b) where 38 monopole equivalent sources are used to match the boundary conditions on each sphere. The rigid boundary surface condition for the diffracting spheres, i.e., zero normal velocity at the sphere surface, is checked at 52 points on the surface of the diffracting sphere.

Figure 8(a) shows the vector plot of the elements of the plant response matrix, assumed to be the nominal plant response $\mathbf{G}_0$ in this study, calculated using ESM without any spheres inside the enclosure. The elements of the plant response have complex values and arrows in the horizontal right-hand direction indicate positive real values and vertical arrows indicate positive imaginary values in all of the vector plots shown in this paper. Figures 8(b)–8(e) show the $\Delta\mathbf{G}$ matrices calculated for the cases shown in Figure 7, which were scaled up by 10 times compared with the plots in Figure 8(a). The changes in the plant response are small for the single-sphere case. When six spheres, or one large sphere with the same total volume, are placed in the enclosure, the changes in the plant response are similar (Figures 8(c) and 8(d)).

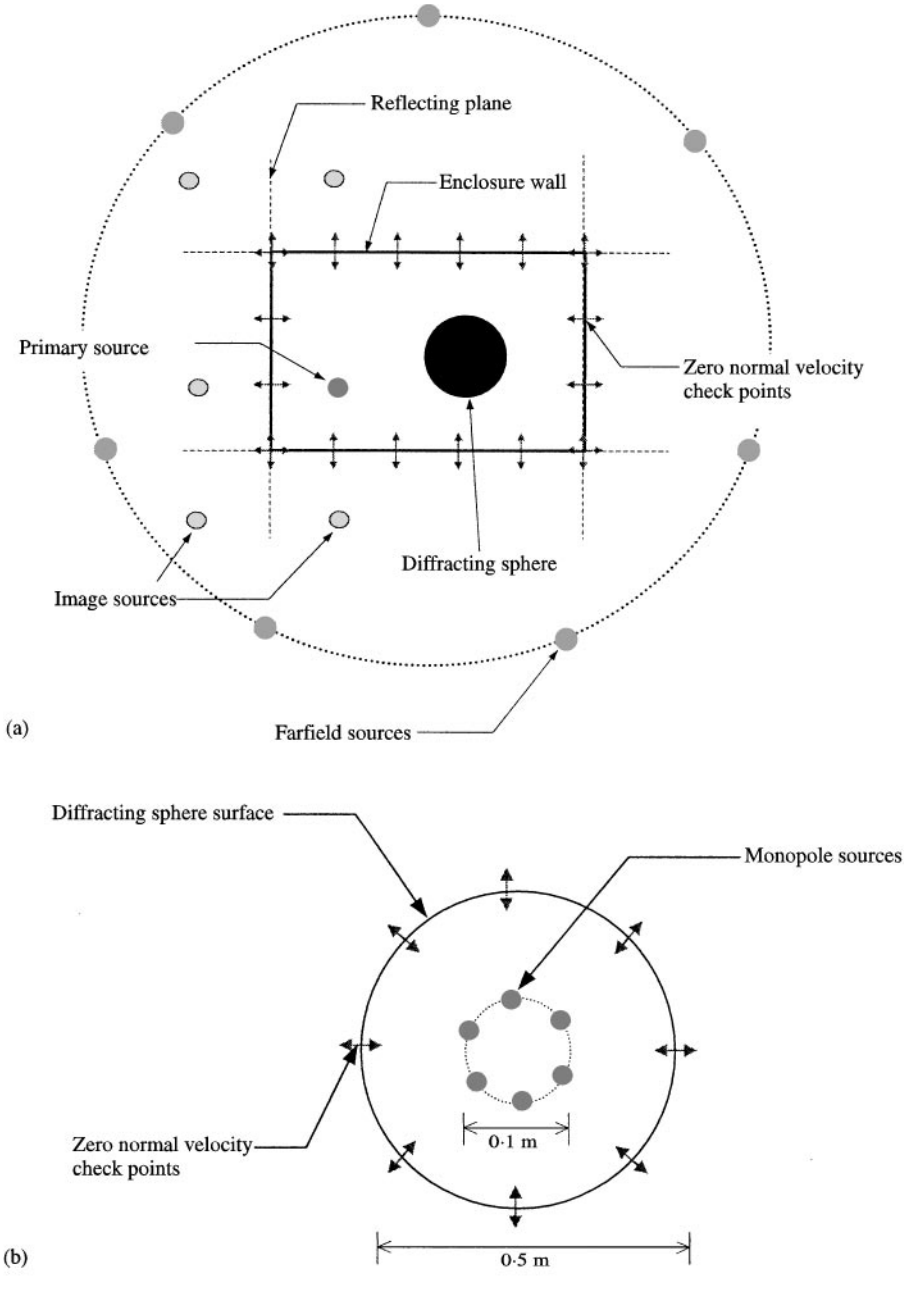

Figure 6. (a) Sketch of ESM modelling for the enclosure and the positions of equivalent sources. (b) Schematic drawing of the sphere model used in ESM calculation.

However, when the six spheres are moved to another position in the enclosure, Figure 8(e), the pattern of the elements in the $\Delta\mathbf{G}$ matrix changes significantly. Note that the form of the $\Delta\mathbf{G}$ matrices is entirely dependent on the ordering of the actuators and sensors assumed in the definition of $\mathbf{G}_0$.

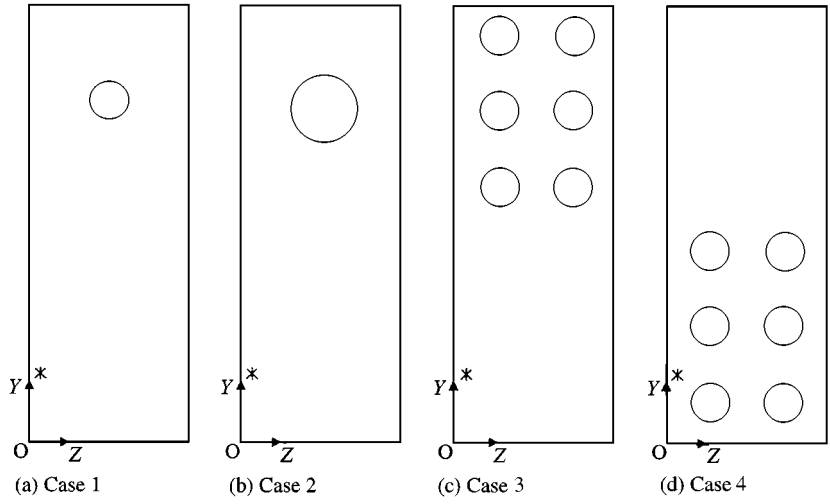

Figure 7. Plan view of internal sphere positions used in the simulation. "$*$" Symbol indicates the approximate position of the primary source.

Whereas Figure 8 shows the effect of the diffracting spheres on the physical plant response matrix, the $\Delta\mathbf{\Sigma}$ matrix defined by equation (62) may be used directly to predict the influence of the uncertainty in the plant response on the performance and stability. Figure 9 shows the structure of the $\Delta\mathbf{\Sigma}$ matrices corresponding to the cases shown in Figure 7, in exactly the same format as was used for the $\Delta\mathbf{G}$ matrices in Figure 8. Figures 9(b)–9(e) show the vector plots of the $\Delta\mathbf{\Sigma}$ matrices for the cases shown in Figures 8(b)–8(e), which are scaled up by 10 or 30 times compared with the $\mathbf{\Sigma}_0$ plot in Figure 9(a). Comparing the cases shown in Figures 9(b) and 9(c), both of which are for the effect of a single sphere but of difference size, the absolute magnitude of $\Delta\mathbf{\Sigma}$ with a single large sphere is much larger than that with single small sphere, but it is interesting to notice that the directions of the arrows, i.e., the ratio of real over imaginary part of each elements in $\Delta\mathbf{\Sigma}$, are now very similar. Figures 9(d) and 9(e) show vector plots of $\Delta\mathbf{\Sigma}$ where there are six diffracting spheres present, but in different positions. It is again interesting to note that the two $\Delta\mathbf{\Sigma}$ matrices now have a very similar form, in contrast to the $\Delta\mathbf{G}$ matrices shown in Figures 8(d) and 8(e). In general, the effects of the diffracting spheres appear in the top left-hand part of the $\Delta\mathbf{\Sigma}$ matrix. From the previous work of Omoto and Elliott [12] this suggests that plant perturbations will have relatively little effect on performance.

The norms of the $\Delta\mathbf{\Sigma}$ matrices for each case, normalized by the norm of $\mathbf{\Sigma}_0$ are summarized in Table 5 which also shows the achievable attenuations ($Attn_p$ and $Attn_\infty$). The norm of the $\Delta\mathbf{\Sigma}$ matrix for case 1 is the smallest since only one sphere is present inside the enclosure and the norm for case 2, with the single large sphere, is largest, about 20% of the nominal value. Compared with $Attn_0$, the attenuation achievable without the diffracting spheres, the attenuation achievable with the spheres present $Attn_p$ show only a fraction of a dB difference, except case 2. This is

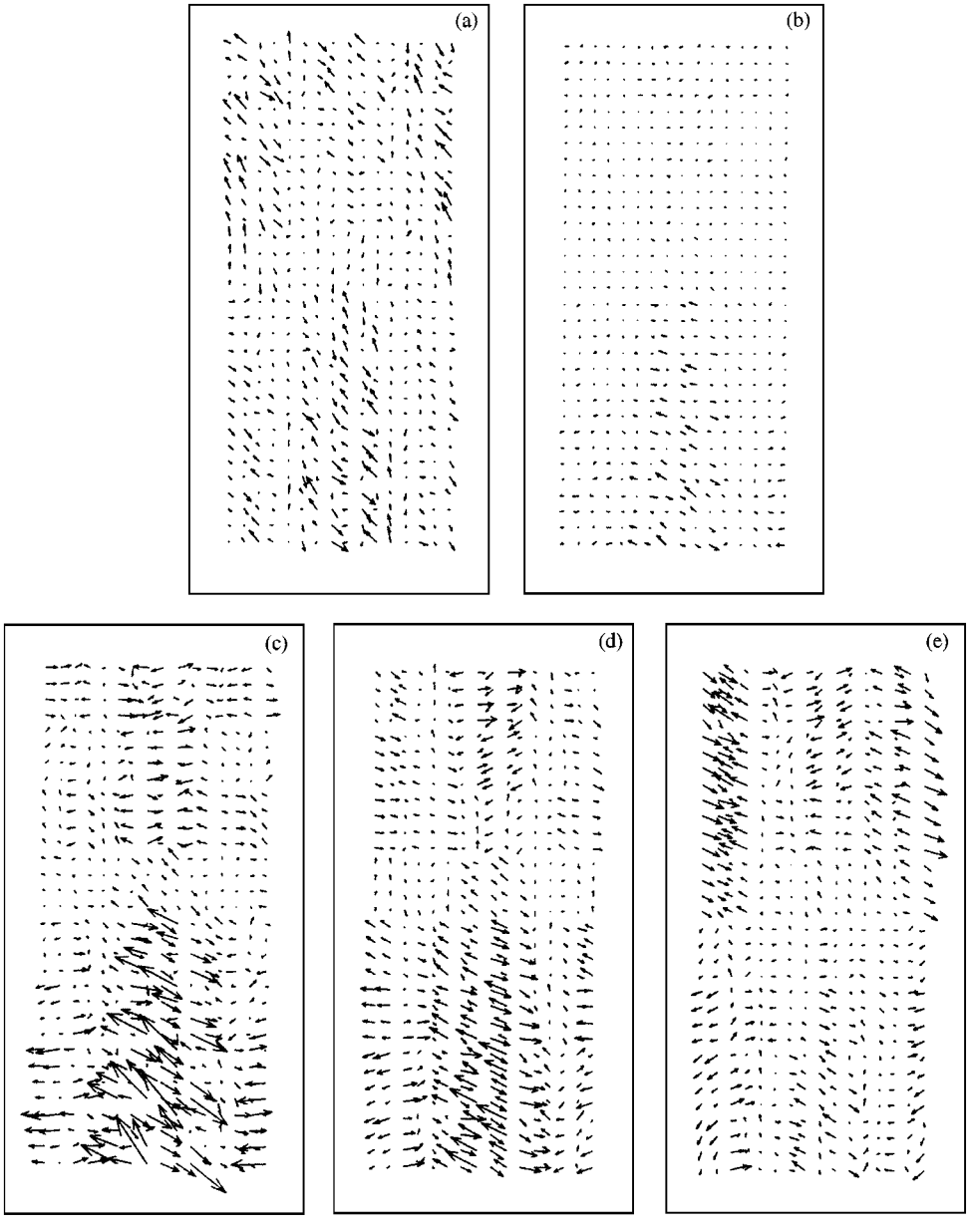

Figure 8. The complex values of the 16×32 elements of the nominal plant response matrix, $\mathbf{G}_0$, and the changes in the plant response matrix, $\Delta\mathbf{G}$, calculated using ESM with and without the spheres for the cases shown in Figure 7. $\Delta\mathbf{G}$ plots are scaled up by 10 times compared with the $\mathbf{G}_0$ plot. (a) $\mathbf{G}_0$ (without sphere); (b) $\Delta\mathbf{G}$ for case 1 (single 0·5 m sphere, Figure 7(a)); (c) $\Delta\mathbf{G}$ for case 2 (single 0·9 m sphere, Figure 7(b)); (d) $\Delta\mathbf{G}$ for case 3 (six 0·5 m spheres, Figure 7(c)); (e) $\Delta\mathbf{G}$ for case 4 (six 0·5 m spheres, Figure 7(d)).

in agreement with Omoto and Elliott [12], who showed that the magnitude of the elements in the lower right-hand side of the $\Delta\mathbf{\Sigma}$ matrix, whose norm is shown to be small in Table 5, will have the greatest effect on the residual error. In fact, the

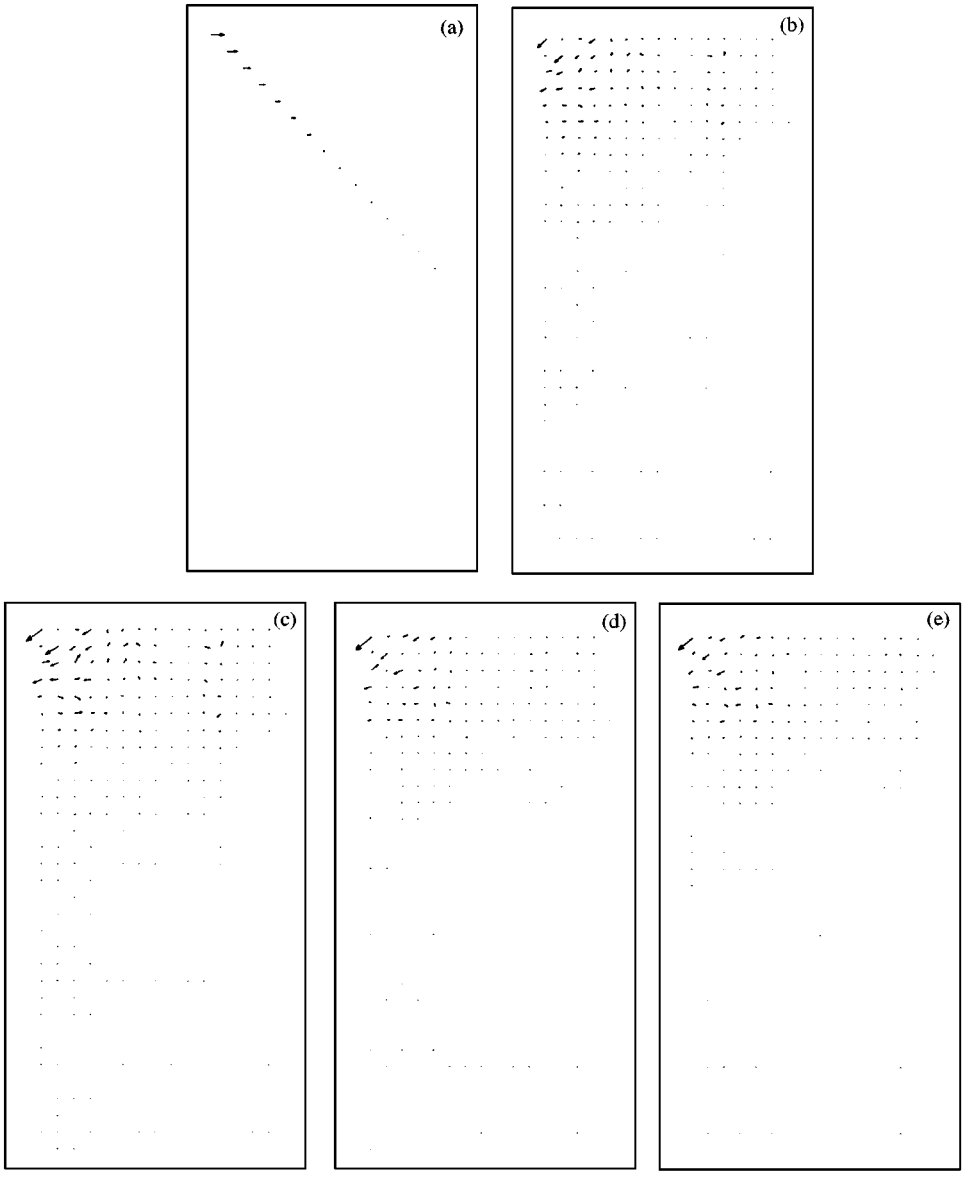

Figure 9. The complex values of the 16×32 elements of the singular value matrix for the nominal plant, $\mathbf{\Sigma}_0$ and the purturbations in the singular value matrix due to plant uncertainty, $\Delta\mathbf{\Sigma}$, for the cases shown in Figure 8. The $\Delta\mathbf{\Sigma}$ plots are scaled up by 30 times in (b) and 10 times in (c)–(e) compared with the $\mathbf{\Sigma}_0$ plot. (a) $\mathbf{\Sigma}_0$ (without sphere); (b) $\Delta\mathbf{\Sigma}$ for case 1 (single 0·5 m sphere, Figure 7(a)); (c) $\Delta\mathbf{\Sigma}$ for case 2 (single 0·9 m sphere, Figure 7(b)); (d) $\Delta\mathbf{\Sigma}$ for case 3 (six 0·5 m spheres, Figure 7(c)); (e) $\Delta\mathbf{\Sigma}$ for case 4 (six 0·5 m spheres, Figure 7(d)).

performance with 6 spheres present is slightly better than when no spheres are present. It is interesting to note that in all cases, the attenuation which could be achieved in an enclosure with spheres, using a control system whose internal model was identified without spheres, $Attn_\infty$, was almost the same as the maximum which could be achieved with an ideal controller in the enclosure with spheres, $Attn_p$.

TABLE 5

Comparison of the norms of $\Delta\mathbf{\Sigma}$ and the attenuations obtained with spheres positioned inside the enclosure as shown in Figure 7

Case	$Attn_p$ (dB)	$Attn_\infty$ (dB)	$\|\Delta\mathbf{\Sigma}\|/\|\mathbf{\Sigma}_0\|$	$\|sub\Delta\mathbf{\Sigma}\|/\|\mathbf{\Sigma}_0\|$
No sphere	43·28	43·28	0·0000	0·00000
1. one 0·5 m	43·07	43·07	0·0447	0·00041
2. one 0·9 m	40·47	40·46	0·2001	0·00156
3. six 0·5 m	43·30	43·30	0·1544	0·00051
4. six 0·5 m	44·10	44·10	0·1348	0·00044

TABLE 6

Average norms and average attenuations calculated using ESM over 20 cases of the plant matrix with 6 and 12 spheres placed randomly in an enclosure

Spheres	$Attn_0$ (dB)	$Attn_p$ (dB)	$Attn_\infty$ (dB)	$\|\Delta\mathbf{\Sigma}\|/\|\mathbf{\Sigma}_0\|$	$\|sub\Delta\mathbf{\Sigma}\|/\|\mathbf{\Sigma}_0\|$
6	43·28	41·69	41·67	0·22815	0·00097
12	43·28	40·87	40·84	0·36630	0·00126

3.2.2. *Averaged performance with 6 and 12 spheres*

Section 3.2.1 described the simulation results with two cases of 6 spheres which are placed in a symmetric pattern. This section describes the effects of 6 and 12 diffracting spheres, but the sphere positions are now randomly selected from a possible 24 locations evenly distributed in a horizontal plane.

A total of 20 sets of 6 or 12 sphere positions are selected and the plant responses were calculated using the ESM for a control system with 32 microphones and 16 loudspeakers. With these 20 sets of $\mathbf{G}_p$ matrices, $\Delta\mathbf{\Sigma}$ matrices are calculated for each case and the averaged values of the norms are summarized in Table 6. Whether 6 or 12 spheres are used, most of the variations appeared on the upper part of the $\Delta\mathbf{\Sigma}$ matrix, as shown in Figure 10, with larger changes in the left-hand side, around the main diagonal elements. This is similar to the pattern in the $\Delta\Sigma$ matrix caused by changes in the primary source excitation frequency described in the work of Omoto and Elliott [12], but is rather different from the variations caused by changes in the positions of the secondary sources or error sensors observed by these authors. The $\Delta\mathbf{\Sigma}$ plots in Figure 10 have strong off-diagonal terms, however, which were not observed for changes in excitation frequency. Clearly, the averaged norm of $\Delta\mathbf{\Sigma}$, and that of the bottom right sub-matrix of $\Delta\mathbf{\Sigma}$, are increased when 12 spheres are used compared with those of 6 spheres, which reflects the fact that more diffracting spheres generate larger uncertainties. The average reduction in performance, however, is only about 1·6 dB with 6 spheres and 2·4 dB with 12 spheres. Whether 6 or 12 spheres are used, the value of $Attn_\infty$ is only marginally smaller than the value of $Attn_p$.

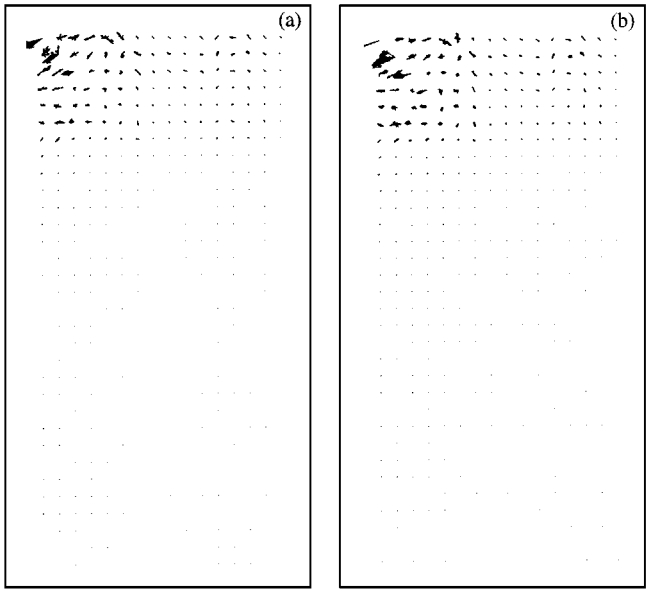

Figure 10. The complex values of the 16×32 elements of the $\Delta\mathbf{\Sigma}$ matrices obtained using ESM calculation with 20 sets of randomly chosen (a) 6 diffracting spheres and (b) 12 diffracting spheres in the enclosure.

The average normalized magnitude of $\Delta\mathbf{\Sigma}$, which is equal to ε_l in equation (7), was about 23% for 6 spheres, but this causes only a 1·6 dB loss of performance in this case. These results can be compared with those of the previous section for unstructured plant uncertainty, which showed that in that case values of ε_1 of only 1% could give rise to reduction of 5 dB in performance. The presence of the spheres can thus be said to have a smaller effect on performance in relation to the sizes of the changes in the plant matrix than random perturbations in the elements of the plant matrix, but these changes are still large enough to motivate choosing loudspeaker locations which are robust to such uncertainties.

3.2.3. *Measured results with diffracting objects*

In order to verify the predicted effects of the diffracting spheres on the $\Delta\mathbf{\Sigma}$ matrix, experiments were carried out with six wooden boxes, which had approximately the same volume as the small spheres modelled above, placed at various positions in an experimental enclosure before the transfer response matrix from each loudspeaker to each microphone was measured. With the 32 microphones and 16 loudspeakers shown in Figure 5, 12 plant responses are measured with the boxes in the enclosure, while changing the box positions randomly for each measurement. The $\Delta\mathbf{\Sigma}$ matrices of the measured results are plotted in Figure 11 which shows that the experimental results have a similar form to those predicted from the ESM calculations. The average norm of $\Delta\mathbf{\Sigma}$ for the measured results is 0·35 which is somewhat larger than the norm of $\Delta\mathbf{\Sigma}$ predicted by the ESM calculations, which was about 0·23. This difference may be due to the different shapes and positions for the diffracting objects, especially in the height within the enclosure. The distance from the centre of

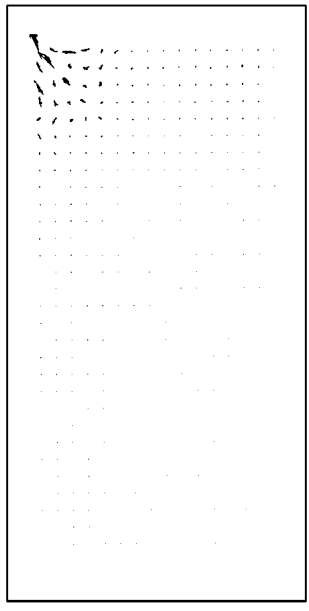

Figure 11. The complex values of the 16×32 elements of 12 $\Delta\mathbf{\Sigma}$ matrices for the plant responses measured with 6 boxes (each box has an equivalent volume of a person) randomly placed in 12 different sets of positions in an enclosure.

the boxes to the floor used in the experiments was about 1·1 m whereas it was 0·75 m for the spheres used in the ESM calculations. The temperature in the enclosure was always around 20°C during the course of the measurements, but small variations in temperature could also have contributed to the measured changes in the $\Delta\mathbf{\Sigma}$ matrix.

4. THE EFFECT OF STRUCTURED UNCERTAINTIES IN TRANSDUCER SELECTION

The optimal transducer positions can be efficiently found using several natural algorithms [5] although the selection of loudspeaker positions is significantly affected by the definition of the fitness function used in the searching algorithm. In this section, we investigate the effect of structured uncertainty in the plant response on the selection of loudspeaker positions. The 20 perturbed plant response matrices, $\mathbf{G}_p$ (32×16), each calculated with six diffracting spheres described in section 3.2.2 together with another set of 20 plant matrices for 16 different loudspeaker positions were used to build plant matrices of dimensions 32×32. A simulated annealing algorithm is then used to select eight optimal loudspeaker positions from the possible 32. In addition to the selection with the plant matrices with structured uncertainty, plant matrices using unstructured uncertainty are also used, which are generated by adding random noise to the nominal plant matrix $\mathbf{G}_0$ calculated from ESM. Based on these two groups of plant response matrices,

four different fitness functions are designed and the performance of each fitness function is compared together in the later part of this section.

4.1. FITNESS FUNCTIONS WITH UNCERTAINTY IN THE PLANT RESPONSE AND DISTURBANCE

Four different fitness functions are defined and tested. As a reference, a fitness function f_1 using the nominal plant response matrix $\mathbf{G}_0$ without uncertainty is defined as

$$f_1 = 10\log_{10}(\mathbf{d}_0^{\mathrm{H}}\mathbf{d}_0/\mathbf{e}_0^{\mathrm{H}}\mathbf{e}_0), \tag{63}$$

where $\mathbf{e}_0$ is given by equation (56). This fitness function is for the case where the plant response is measured for the empty enclosure and the physical plant response remains unchanged during the control.

The second case is where the plant responses and primary disturbances are calculated with the diffracting spheres in the enclosure, which generates structured uncertainty. The matched plant response matrix $\mathbf{G}_p$ and the primary disturbance vector $\mathbf{d}_p$ calculated with 20 different examples of six diffracting spheres are used in the fitness function f_2 which is defined as

$$f_2 = 10\log_{10}(\sum\mathbf{d}_p^{\mathrm{H}}\mathbf{d}_p/\sum\mathbf{e}_p^{\mathrm{H}}\mathbf{e}_p), \tag{64}$$

where $\mathbf{e}_p$ is given by equation (57) and the sum is taken over all 20 cases. The plant response matrix $\mathbf{G}_p$ is used here as both the estimated plant response and physical plant response.

In the third case, plant responses with unstructured uncertainties are used. A total of 20 plant response matrices were generated by adding random noise to the nominal plant response $\mathbf{G}_0$ and the fitness function f_3 for this case is defined as

$$f_3 = 10\log_{10}(20\cdot\mathbf{d}_0^{\mathrm{H}}\mathbf{d}_0/\sum\mathbf{e}_p^{\mathrm{H}}\mathbf{e}_p). \tag{65}$$

In the last case, the fitness function uses plant response matrices which have both structured and unstructured uncertainties. The plant response matrices with structured uncertainty used in the fitness function f_2 are again used, but random noise is now added to also give a degree of unstructured uncertainty in the plant responses. Therefore, the fitness function f_4 is defined as

$$f_4 = 10\log_{10}(\sum\mathbf{d}_p^{\mathrm{H}}\mathbf{d}_p/\sum\mathbf{e}_p^{\mathrm{H}}\mathbf{e}_p), \tag{66}$$

where $\mathbf{d}_p$ represents the matched primary disturbance vector without unstructured uncertainty and $\mathbf{e}_p$ represents the error signal with the plant response matrix calculated with spheres, together with unstructured uncertainty of $\varepsilon_l = 0{\cdot}6\%$.

The results of the selection using the fitness function f_1 indicate that some of the loudspeaker configurations require significantly higher control effort than others. These configurations are the cases we would not want to choose. The results of the

TABLE 7

Averaged attenuation and control effort (in parentheses) achievable with the loudspeaker positions found with four simulated annealing searches, each conducted using a different fitness function. The fitness functions are with no uncertainty, f_1, with uncertainty due to the presence of spheres in the enclosure, f_2, with uncertainty due to random perturbations of the plant matrix, f_3, and with both types of uncertainty, f_4. Twenty sets of loudspeaker positions from the results of each search are then used to evaluate the performance using each of the fitness functions

Fitness function used in the search	Functions used in the evaluation			
	f_1	f_2	f_3	f_4
f_1 (nominal)	**44·39** **(12·21)**	35·76 (6·81)	37·41 (1·20)	34·02 (1·29)
f_2 (structured)	41·39 (0·63)	**39·06** **(0·65)**	39·27 (0·63)	37·78 (0·65)
f_3 (0·6% unstructured)	42·56 (0·62)	36·99 (0·65)	**40·13** **(0·61)**	36·18 (0·64)
f_4 (structured + 0·6% unstructured)	41·29 (0·57)	38·98 (0·59)	39·41 (0·57)	**37·86** **(0·59)**

selection using the fitness function f_2, f_3 and f_4 effectively filter out such configurations, although they also show a different performance in the attenuation under different conditions. Table 7 shows the average attenuations and control efforts when the best 20 sets of loudspeaker positions found with the selection using each of the four fitness functions are used to calculate the average performance in each of the four cases. Clearly, the loudspeaker positions found with one fitness function perform best when they are evaluated in the same way. The positions found with the fitness function f_1 (nominal) performs the best when evaluated with f_1 for example, but for all the other fitness functions this is the worst performer in terms of both of the attenuations and control efforts.

The next worst case can be seen from the results obtained using f_3 in the search, which is the case of having purely unstructured uncertainty in the plant response. The loudspeaker positions found with this fitness function perform fairly well when they are used in the empty enclosure, without any uncertainties, but the attenuation drops by about 4 dB when used in the mixed uncertainty environment (f_4). The performance when searching with fitness function f_2, with structured uncertainties, was about 2 dB better than when the loudspeaker selection was made assuming only unstructured uncertainty and 3 dB better than when the loudspeaker selection was made assuming no uncertainty. This ranking is not affected by the presence of additional unstructured uncertainty in the fitness function (f_4).

The control effort is relatively low with the loudspeaker positions found using the fitness function f_2, f_3 or f_4, which indicates that the inclusion of any uncertainties in the fitness function effectively prevents the selection of loudspeaker positions which give rise to ill-conditioned control problems.

4.2. FITNESS FUNCTIONS WITH SYNTHETIC $\Delta\boldsymbol{\Sigma}$ MATRICES

The fitness functions used in section 4.1 required plant responses and disturbances calculated using the ESM model. The calculations of these plant responses and disturbances can be very expensive computationally, depending on the number of diffracting object and shapes, for example. Instead of using such computationally expensive methods, it may be possible to use the structure of the $\Delta\boldsymbol{\Sigma}$ matrix observed for the ESM simulations to generate an ensemble of candidate plant responses for the loudspeaker selection from a single nominal plant response matrix.

It is assumed that the effect of structured uncertainty mainly appears on the upper left part of $\Delta\boldsymbol{\Sigma}$ matrix. The magnitude of each element in the $\Delta\boldsymbol{\Sigma}$ matrix with the structured uncertainty is assumed to be inversely proportional to the distance from the top left element, the largest singular value, but the phase of the element is assumed to be random. Therefore, if an approximate value of the largest singular value of the $\Delta\boldsymbol{\Sigma}$ matrix is known we can easily generate a synthetic ensemble of plant response matrices with uncertainties. This technique could also be used to generate a set of perturbed plant responses from a single measured response.

Searches for loudspeaker positions were performed using these synthetic plant responses with four different fitness functions and the average performance of the loudspeaker sets selected using each fitness function is compared in Table 8. Fitness function f_1, defined in equation (63), is again used here as a reference. Fitness function f_a uses a single plant response generated from the average of 20 $\Delta\boldsymbol{\Sigma}$ matrices obtained using ESM with six diffracting spheres. Fitness function f_b is very similar to f_2 defined in equation (64) and uses the errors evaluated from plant matrices calculated using the ESM method, but uses the nominal disturbance $\mathbf{d}_0$ instead of $\mathbf{d}_p$. Fitness function f_c uses the synthetic ensemble of plant response generated in the way described in this section.

Table 8 shows that the positions found with the fitness function f_1 performs well when evaluated with f_1 but for all the other fitness functions the performance is very poor, with control efforts which are significantly higher than those of all the other fitness functions. The positions found using fitness function f_a perform well for the nominal plant response but have poor performance for the other cases with considerably high control efforts. The positions found using fitness function f_b and f_c show very similar performance, with high attenuation and low control effort. This indicates that the synthetically generated plant responses can be used instead of those generated using a complete simulation to select good loudspeaker positions whose performance is robust to structured uncertainty.

5. CONCLUSIONS

The effects of uncertainty in the plant response and disturbance on the performance of an active control system have been studied, particularly related to the placement of transducers. Two cases have been considered, with either structured or unstructured uncertainty.

TABLE 8

Averaged attenuation and control effort (in parentheses) achievable with the loudspeaker positions found with four simulated annealing searches, each conducted using a different fitness function. The fitness functions are with no uncertainty and the plant response with no spheres, f_1, with no uncertainty and the average plant response with spheres, f_a, with uncertainty due to the presence of spheres in the enclosure, f_b, and with uncertainty due to random numbers in the elements of the $\Delta\boldsymbol{\Sigma}$ matrix whose magnitudes were similar to those due to the presence of spheres. Twenty sets of loudspeaker positions from the results of each search are then used to evaluate the performance using each of the fitness functions

Fitness function used in the search	Functions used in the evaluation			
	f_1	f_a	f_b	f_c
f_1 (nominal)	**44·39** **(12·21)**	19·99 (1·20)	25·58 (21·74)	26·89 (2·67)
f_a ($\boldsymbol{\Sigma}_0 + \overline{\Delta\boldsymbol{\Sigma}}$)	36·18 (3·10)	**26·56** **(1·42)**	24·46 (8·07)	25·37 (1·32)
f_b (6 sphere, ESM)	38·36 (0·55)	17·76 (0·70)	**37·28** **(0·81)**	33·48 (0·57)
f_c (synthetic)	38·41 (0·57)	17·44 (0·77)	36·06 (0·96)	**33·81** **(0·61)**

For the unstructured uncertainty in the plant response and disturbance, the performance could be derived analytically using the assumed statistical property of the uncertainty. A particularly simple analytic form could be derived for unstructured uncertainties in the disturbance, which indicates that the resultant additional residual error is independent of the particular choice of actuator positions but depends only on the level of uncertainty and the relative numbers of actuators and sensors. Theoretical analysis of the performance with unstructured uncertainty in the plant response shows that the loudspeaker positions which give good attenuation with low control effort will generally be robust to such uncertainty. The performance of practical systems is largely dominated by uncertainty in the plant response, so that the results with combined uncertainties are primarily affected by the uncertainty in the plant response if both have the same level of uncertainty. In general, whether the uncertainty is in the plant response or disturbance or both, the loudspeaker position sets with low control effort give consistently good attenuations. Such positions have been identified using a simulated annealing search using the fitness function which measures average performance over several sets of plant responses and disturbances.

The effects of structured uncertainty have been analyzed by considering the changes to the singular-value matrix, $\Delta\boldsymbol{\Sigma}$, of the plant response. The structured uncertainty in the plant response is assumed to be generated by the presence of diffracting spheres inside an enclosure. Using the equivalent source method, plant response matrices have been generated with and without the diffracting spheres.

Experiments were also performed to measure the plant responses with box-shaped objects inside an enclosure. The vector plots of the measured $\Delta\boldsymbol{\Sigma}$ matrices are compared with those calculated using the ESM and found to have similar patterns. The results indicate that this kind of uncertainty has a characteristic pattern in the vector plots, although it is fairly similar to that caused by changes in the excitation frequency.

The effect of structured uncertainty on the selection of optimal loudspeaker positions was also studied. Twenty sets of plant response matrices with structured uncertainty were generated using the ESM in an enclosure with 6 or 12 randomly positioned spheres present. Several fitness functions are tested using these plant response matrices with structured and unstructured uncertainties. For each of the fitness functions, the best 20 sets of 8 loudspeaker positions are selected from a possible 32 locations and the averaged performance is evaluated for various situations. In general, the loudspeaker sets chosen using the fitness functions based on the plant response matrices with structured uncertainty show better performance than the others, showing fairly consistent performance under a variety of evaluation conditions. Whether the uncertainty is structured or unstructured, the loudspeaker positions chosen effectively discriminated against loudspeaker positions sets which required a high control effort.

ACKNOWLEDGMENTS

This work has been supported by the TNO Institute of Applied Physics, The Netherlands, and helpful discussions with Dr N. J. Doelman are gratefully acknowledged.

REFERENCES

1. S. S. Rao and T.-S. Pan 1991 *AIAA Journal* **29**, 942–943. Optimal placement of actuators in actively controlled structures using genetic algorithms.
2. J. Onoda and Y. Hanawa 1993 *AIAA Journal* **31**, 1167–1169. Actuator placement optimisation by genetic and improved simulated annealing algorithms.
3. D. T. Tsahalis, S. K. Katsikas and D. A. Manolas 1993 *Proceedings Inter-Noise* '93, *Leuven*, 83–88. A genetic algorithm for optimal positioning of actuators in active noise control: results from the ASANCA project.
4. E. Benzaria and V. Martin 1994 *Journal of Sound and Vibration* **173**, 137–144. Secondary source location in active noise control: selection or optimisation?
5. K.-H. Baek and S. J. Elliott 1995 *Journal of Sound and Vibration* **186**, 245–267. Natural algorithms for choosing source locations in active control systems.
6. H. Hamada, N. Takashima and P. A. Nelson 1995 *Proceedings ACTIVE* '95, *the International Symposium on Active Control of Sound and Vibration*, 33–37. Genetic algorithms used for active control of sound—search and identification of noise sources.
7. M. T. Simpson and C. H. Hansen 1996 *Noise Control Engineering Journal* **44**, 169–184. Use of genetic algorithms to optimise vibration actuator placement for active control of harmonic interior noise in a cylinder with floor structure.
8. C. C. Boucher, S. J. Elliott and K.-H. Baek 1996 *Proceedings InterNoise* '96, *Liverpool, U.K.* 1179–1182. Active control of helicopter rotor tones.

9. K.-H. Baek and S. J. Elliott 1997 *Digest of IEE Colloquium on Active Sound and Vibration Control, London*, 97/385, 3/1–3/5. Unstructured uncertainty in transducer selection for multichannel active control systems.
10. M. E. Johnson, S. J. Elliott, K.-H. Baek and J. Garcia-Bonito 1998 *Journal of the Acoustical Society of America* **104**, 1221–1231. An equivalent source technique for calculating the sound field inside an enclosure containing scattering objects.
11. V. Martin and C. Gronier 1998 *Journal of Sound and Vibration* **215**, 827–852. Minimum attenuation guaranteed by an active noise control system in presence of errors in the spatial distribution of the primary field.
12. A. Omoto and S. J. Elliott 1997 *IEEE Transactions on Speech and Audio Processing* **7**, 204–212. The effects of structured uncertainty in the acoustic plant on multichannel feedforward control systems.